Biophysical Chemistry 149 (2010) 47–57

Contents lists available at ScienceDirect

Biophysical Chemistry

journal homepage: http://www.elsevier.com/locate/biophyschem

Excited protein states of human tear lipocalin for low- and high-affinity ligand binding revealed by functional AB loop motion

Oktay K. Gasymov *, Adil R. Abduragimov, Ben J. Glasgow *

Department of Pathology, University of California at Los Angeles, United States
Department of Ophthalmology and Jules Stein Eye Institute, University of California at Los Angeles, United States

ARTICLE INFO

Article history:
Received 24 February 2010
Received in revised form 22 March 2010
Accepted 28 March 2010
Available online 9 April 2010

Keywords:
Excited protein states
Ligand binding
Tear lipocalin
Protein dynamics
FRET

ABSTRACT

Human tear lipocalin (TL), a prominent member of lipocalin family, exhibits functional and structural promiscuity. The plasticity of loop regions modulates entry to the ligand pocket at the "open" end of the eight-stranded β-barrel. Site-directed multi-distance measurements using fluorescence resonance energy transfer between functional loops register two excited protein states for low- and high-affinity ligand binding. At low pH, the longest loop AB adopts the conformation of the low-affinity excited protein state that matches the crystal structure of holo-TL at pH 8. A "crankshaft" like movement is detected for the loop AB in a low pH transition. At pH 7.3 the holo-protein assumes a high-affinity excited protein state, in which the loop AB is more compact (RMS = 3.1 Å). In the apo-holo transition, the reporter Trp 28 moves about 4.5 Å that reflects a decrease in distance between Glu27 and Lys108. This interaction fixes the loop AB conformation for the high-affinity mode. No such movement is detected at low pH, where Glu27 is protonated. Data strongly indicate that the protonation state of Glu27 modulates the conformation of the loop AB for high- and low-affinity binding.

1. Introduction

Tear lipocalin (TL), also known as lipocalin 1, Lcn1, von Ebner's gland protein, belongs to the lipocalin family [1]. The first structural data on TL, determined by site-directed tryptophan fluorescence (SDTF), have revealed a typical lipocalin fold. The solution structure has demonstrated a capacious ligand binding barrel that consists of eight antiparallel β-strands with a repeated +1 topology [2]. These findings have subsequently been confirmed by X-ray crystallography of TL [3].

TL is the principal lipid binding protein in tears. Endogenous ligands of TL include an assortment of fatty acids, alkyl alcohols, glycolipids, phospholipids and cholesterol [4]. In addition, TL binds numerous synthetic ligands [4–7]. TL has diverse functions, each of which could be physiologically significant in human tears. Included are scavenging lipid from the corneal surface to prevent the formation of lipid induced dry spots [8,9], solubilization of lipid in tears [2], antimicrobial activity [2,10,11], cysteine proteinase inhibition [12], transport of sapid molecules in saliva [13], transport of retinol in tears [14], scavenging potentially harmful lipid oxidation products [15], transport of antioxidants in tears [16], and endonuclease activity [17,18].

The ability to bind the various classes, sizes and shapes of ligands, makes TL a perfect paradigm for drug delivery. The lipocalin scaffold has successfully been engineered to achieve predetermined unique or double ligand specificities [19–21]. These proteins were classified as anticalins and duocalins, respectively. The molecular basis of ligand binding by TL is critical to understand its functional capacity in different environments. Bound fatty acids are predominantly oriented with the hydrocarbon tail buried in the cavity and the carboxyl group oriented toward the mouth [22,23]. However, relatively weak binding in the reverse orientation may stabilize the lipid layer of tears [24–26]. SDTF has been applied to ligand binding. In solution the ligand does not have a unique position but is distributed in the cavity of TL. The binding energy landscape reveals an asymmetric distribution of ligand positions in the cavity [27].

Residues in the loops AB and GH of TL are directly involved in ligand binding and may modulate the binding event [27]. In an independent study [28], the newly resolved crystal structure of TL in holo-form (with the artificial ligand 1,4-butanediol) shows major conformational changes in the loops AB, CD, and GH at the open end of the cavity.

TL as well as some other lipocalins, such as retinol binding protein [29,30], nitrophorin [31], and the membrane enzyme PagP [32], shows pH-dependent ligand binding. However, the molecular mechanism of action is unique for each lipocalin. Low pH induces structural rearrangements in TL that influence ligand binding [5,33–35]. The tear

* Corresponding authors. Gasymov is to be contacted at 100 Stein Plaza, Rm# B267, Los Angeles, CA 90095, United States. Tel.: +1 310 825 6261; fax: +1 310 794 2144. Glasgow, 100 Stein Plaza, Rm# B269, Los Angeles, CA 90095, United States. Tel.: +1 310 825 6998; fax: +1 310 794 2144.
E-mail addresses: ogassymov@mednet.ucla.edu (O.K. Gasymov), bglasgow@mednet.ucla.edu (B.J. Glasgow).

0301-4622/$ – see front matter © 2010 Elsevier B.V. All rights reserved.
doi:10.1016/j.bpc.2010.03.017

film lipid layer is rich with negatively charged lipids and can potentially create a low pH gradient across the lipid–water interface [36]. In vitro, TL interacts and stabilizes the lipid layer [8,25]. Therefore, the function of TL at low pH is germane to the physiology of tears.

The conformational rearrangements, mainly involving the loops at the open end of the calyx, are proffered as a general feature of the ligand binding mechanism of the lipocalins [37]. In TL, low pH induces the conformational changes that result in decreased distance between the loops CD and EF [34]. However, the conformational state of the loop AB is regulated by the electrostatic interaction between the residues of the adjacent loops AB and GH [28,38]. Therefore, the details of the movements of these loops induced by low pH hold considerable interest.

In this study, SDTF in combination with FRET was used to probe the movements of the loops AB and GH in apo-holo transition at pH values of 3.0 and 7.3. Multi-distance measurements show that pH induced conformational changes are linked to a sizable movement of the functional loop AB. These data indicate that the electrostatic interaction between the residues Glu27 (loop AB) and Lys108 (loop GH) sets the conformation of the loop AB for high-affinity mode. At low pH, protonation of Glu27 disrupts the electrostatic interaction and triggers the movement of the loop AB to the low-affinity mode.

2. Materials and methods

Dansylamidoethyl methanethiosulfonate (MTS-dansyl) was purchased from TRC Inc (North York, Ontario, Canada). N-acetyl-L-tryptophanamide (NATA) and other chemicals used to prepare various buffers were purchased from Sigma-Aldrich (St. Louis, MO).

2.1. Site-directed mutagenesis and plasmid construction

The TL cDNA in PCR II (Invitrogen), [39], was used as a template to clone the TL gene spanning bases 115–592 of the previously published sequence [14] into pET 20b (Novagen, Madison, WI). Flanking restriction sites for NdeI and BamHI were added to produce the native protein sequence as found in tears but with the addition of an initiating methionine [40]. To monitor low pH induced movement of the loops AB and GH, Trp–dansyl pairs (donor and acceptor, respectively) were introduced to TL for RET measurements. To avoid disulfide scrambling with the adjacent Cys61–Cys153 bond during the folding, the residues of the loop AB (26–37) and GH (105) were sequentially substituted with Trp rather than a cysteine (dansyl labeling). To prevent the distortion of the electrostatic potential as well as the conformation, the residues Arg26, Glu27, Pro29, Glu30 and Glu34 were excluded from the Trp substitution experiment. In each single Trp mutant, the residue 81 (or in two instances 78 of β-strand E) in the loop EF was substituted with Cys and then labeled with dansyl group to use as an acceptor in RET.

To construct mutant proteins with a single tryptophan–cysteine pair, the previously well characterized TL mutant, W17Y/C101L, was prepared with oligonucleotides (Universal DNA Inc., Tigard, OR) by sequential PCR steps [7,41]. This mutant was used as a template for subsequent mutations. Amino acid 1 corresponds to His, bases 115–118 according to Redl [14]. Mutants that have both a single Trp and a single Cys additional substitution include: F28W/G81C (for simplicity W28C81); M31W/G81C (W31C81); N32W/T78C(W32C78); N32W/G81C (W32C81); L33W/G81C (W33C81); S35W/G81C (W35C81); V36W/G81C (W36C81); T37W/G81C (W37C81); L105W/T78C (W105C78); and L105W/G81C (W105C81).

2.2. Expression and purification of mutant proteins

E. coli, BL 21 (DE3), were transformed with the mutant plasmids and cells were cultured and proteins were expressed, purified, and analyzed as described in the supporting information [2,34]. The expressed mutant proteins were used as apo-proteins to ensure proper comparison with the crystal structure of apo-TL [3]. Apo-TL was saturated with palmitic acid (1:2) to obtain holo-TL.

2.3. Absorption spectroscopy

UV absorption spectra were measured at room temperature using Shimadzu UV-2400PC spectrophotometer. To ensure the accuracy in quantum yield calculations, the spectra were corrected for scattering by plotting the log of absorbance of the solution versus the log of the wavelength and extrapolating the linear dependence between these quantities in the range 330–390 nm to the absorption range 240–330 nm.

2.4. CD spectral measurements and secondary structure analysis

Far-UV spectra were recorded (Jasco 810 spectropolarimeter, 0.2 mm path length) using a protein concentration of 1.2 mg/ml. Eight scans from 190 to 260 nm were averaged. CD spectra were recorded in mdegrees and converted to mean residue ellipticity in $\mathrm{deg\,cm^2\,dmol^{-1}}$.

CD spectra of TL mutants at pH values of 7.3 and 3.0 were analyzed to calculate the content of secondary structure utilizing a CDPro program with three algorithms: CONTINLL, CDSSTR, and SELCON3 [42]. SMP56, which includes 56 proteins, was used as the protein reference set. The normalized root-mean-square deviation (nrmsd) values between the experimental and calculated spectra were used to judge the goodness of fit. The nrmsd was calculated as:

$$nrmsd = \sqrt{\frac{\sum_N \left(\Delta\theta_{exp} - \Delta\theta_{calc}\right)^2}{\sum_N \left(\Delta\theta_{exp}\right)^2}}$$

where $\Delta\theta_{exp}$ and $\Delta\theta_{calc}$ are the experimental and calculated mean residue ellipticity, respectively. N is the number of data points.

2.5. Fluorescence labeling of TL mutants

Labeling of each TL mutant was carried out by using a 5× molar excess of the fluorescent label (MTS-Dansyl) in buffer 10 mM NaP, pH 6.8 at 4 °C overnight. Free label was separated from the labeled protein by gel filtration on a desalting column (Pharmacia Biotech HiTrap, 5 mL) or Centricon 10 (Amicon, Inc.). Absorption spectra were used to calculate the labeling efficiency for each mutant. Concentrations were calculated using the extinction coefficient $\varepsilon_{335} = 4100\ \mathrm{M^{-1}\,cm^{-1}}$ for MTS-Dansyl. For fluorescence measurements, the buffer of the protein solution was replaced with 10 mM sodium phosphate (pH 7.3) or 30 mM sodium citrate (pH 3.0) using Centricon 10. The protein concentration was determined by the biuret and Lowry (for dilute solution) methods. The efficiencies of labeling for all considered TL mutants were in the range of 0.64–1.22.

2.6. Steady-state fluorescence spectroscopy

Steady-state fluorescence measurements were made on a Jobin Yvon-SPEX (Edison, NJ). Fluorolog tau-3 spectrofluorometer bandwidths for excitation and emission were 2 nm and 3 nm, respectively. The excitation λ of 295 nm was used to ensure that light was absorbed almost entirely by tryptophanyl groups. Protein solutions with about 0.05 OD at 295 nm were analyzed. All spectra were obtained from samples in 10 mM sodium phosphate (pH 7.3) or 30 mM sodium citrate (pH 3.0). The fluorescence spectra were corrected for light scattering from buffer and the instrument response using the appropriate correction curve. The quantum yields of single Trp

mutants were calculated using NATA as a fluorescence standard. The quantum yield of NATA in water was taken to be 0.13 [43]. To improve accuracy in calculations of the quantum yields as well as the overlap integrals (see below), the blue side of the emission spectra was constructed using the log-normal function as described previously [34].

2.7. Fluorescence lifetime measurements

Time-resolved intensity decay data were obtained using a HORIBA Jobin Yvon MF^2 phase/modulation multi-frequency-domain fluorometer. The excitation wavelength was 295 nm from LED-295. Emission was detected through a combination of filters (Semrock LP02-325RS-25 and Corning 7–51), which provides a bandpass of 325–410 nm. The available frequency range was 0.1–310 MHz. P-terphenyl in ethanol was used as a reference standard ($\tau = 1.05$ ns). Data analyses were performed with nonlinear least-squares programs from the Center for Fluorescence Spectroscopy (M. L. Johnson), University of Maryland at Baltimore, School of Medicine (Baltimore, MD). The goodness of fit was assessed by the χ^2 criterion.

The intensity decay data were analyzed in terms of the multi-exponential decay law:

$$I(t) = \sum_i \alpha_i \exp(-t/\tau_i)$$

where α_i and τ_i are the normalized preexponential factor and decay time, respectively. The fractional fluorescence intensity of each component is defined as $f_i = \alpha_i\tau_i / \sum_j f_j\tau_j$.

Mean lifetime (intensity averaged) was calculated as $\tau_{av} = \sum_i f_i\tau_i$. However, the amplitude-averaged lifetime, $\langle\tau\rangle = \sum_i \alpha_i\tau_i$, was used for the calculation of efficiency of RET [44,45]. The radiative rate constant was calculated as $k_r = Q/\langle\tau\rangle$. The fluorescence lifetime data represent the average of at least 3 independent experiments, each of which is the average of 5 to 7 measurements.

All single Trp mutant proteins, except W37C81, showed lower average fluorescence lifetimes at pH 3.0 compared to that of pH 7.3. The effects of reshuffling between the rotamer populations were distinguished from dynamic quenching by the following formula [34,46]:

$$\frac{\langle\tau\rangle}{\langle\tau_0\rangle} = \frac{\sum \alpha_i\tau_{0i}}{\sum \alpha_{0i}\tau_{0i}} \times \frac{\sum \alpha_i\tau_i}{\sum \alpha_i\tau_{0i}} = f_{PR} \times f_{DQ}$$

where subscript 0 refers to the reference state (lifetime parameter at pH 7.3), f_{PR} and f_{DQ} represent population reshuffling and pure dynamic quenching, respectively. All resolved fluorescence lifetimes fall into three groups, 0.22–0.63 ns, 0.86–2.72 ns and 2.86–9.02 ns (see below). Therefore, the parameters were calculated from three lifetime components. The parameter (f_{PR} or f_{DQ}) most deviated from unity plays the dominant role in changes of the fluorescence lifetimes.

2.8. Distance measurements by RET

Resonance energy transfer between the Trp residue (donor) and the labeled dansyl group (acceptor) was used to determine average distance in different conditions. The efficiency of RET, E, can be calculated from

$$E = 1 - \frac{\langle\tau_{DA}\rangle}{\langle\tau_D\rangle}; E_{corr} = \frac{E}{f_a}$$

where $\langle\tau_{DA}\rangle$ and $\langle\tau_D\rangle$ are the fluorescence lifetimes of the donor in the presence and absence of acceptor, respectively. f_a is the fraction of dansyl labeling. E_{corr} is the efficiency of RET corrected for incomplete labeling of the acceptor. In analysis, the dansyl group was assumed not to interfere with the conformation of the tryptophan residue. In two instances, to check the accuracy of the distance measurements, the residue 78 (instead of 81) on the β-strand E was substituted with Cys for dansyl labeling. The side chain of the residue 78 is directed outside the cavity (Fig. 1) and, therefore, susceptible for dynamic random averaging for the donor–acceptor pair.

It should be mentioned that although the same Cys81 is used for dansyl labeling in various single Trp mutants, the labeling efficiencies are different for some of them. This partially could be rationalized by oxidation of –SH groups during the protein expression. Because of native –S–S– bond, the standard treatment with a thiol-reducing agent (e.g., dithiothreitol) prior to the labeling was not used. To avoid unspecific labeling, the incubation time for the labeling was not increased.

According to Förster's theory [47], the efficiency of RET, E, between a donor, D, and an acceptor, A, is given by

$$E = \frac{R_0^6}{R_0^6 + R^6}$$

where R is the distance between the donor and the acceptor. The Förster distance, R_0 (in angstroms) at which 50% energy transfer occurs is obtained from

$$R_0^6 = 8.79 \times 10^{-5}\left[\kappa^2 n^{-4} \phi_D J(\lambda)\right].$$

The refractive index, n, of the medium is taken to be 1.5 [45]. φ_D is the quantum yield of the donor in the absence of the acceptor. Because distance measurements were applied to loop regions, the orientation factor, κ^2, was assumed to be 2/3, which is appropriate for dynamic random averaging of the donor and acceptor.

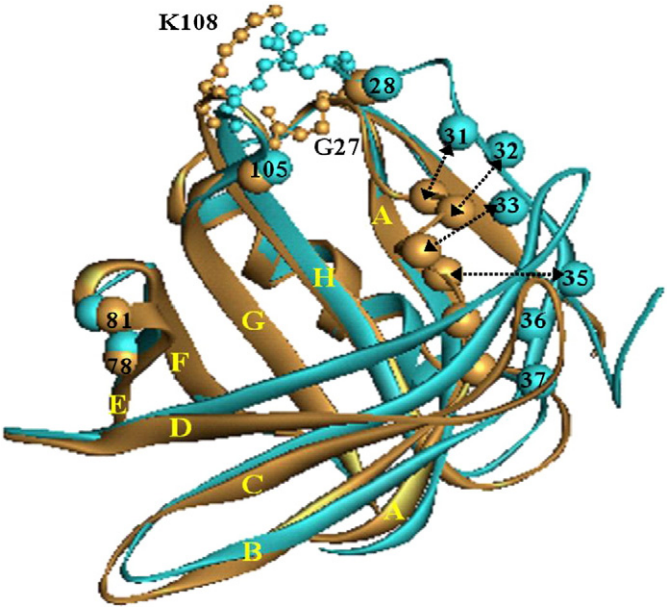

Fig. 1. Ribbon diagrams of the crystal structures of TL in apo- (dark goldenrod) and holo-forms (cyan). The residues in loops AB (28–37) and GH (105) were sequentially substituted with Trp to use as donors in RET experiments. The residues in loop EF (81 and 78) were sequentially substituted with Cys, then labeled with dansyl groups, to use as acceptors. Large-sized balls show locations of the C^{α} atoms. The identical residues in apo- and holo-forms are indicated with double-headed arrows. Side chain residues K108 and E27 (electrostatic interaction) are shown in stick and ball representations. Single capital letters denote the identities of the β-strands that comprise the ligand binding barrel. The ribbon diagrams of apo-TL and holo-TL were generated from PDB files, 1XKI and 3EYC, respectively, with DS Visualizer 2.5 (Accelrys Inc.).

The overlap integral $J(\lambda)$ (in $M^{-1}\,cm^{-1}\,nm^4$) that represents the degree of the spectral overlap between the emission spectrum of the donor $F_D(\lambda)$ and the absorption spectrum of the acceptor $\varepsilon_A(\lambda)$ is defined as

$$J(\lambda) = \frac{\int F_D(\lambda)\varepsilon_A(\lambda)\lambda^4 d\lambda}{\int F_D(\lambda) d\lambda}.$$

3. Results

The residues selected for distance determinations between the loops in the open end of the binding barrel of TL are shown in Fig. 1. The loop AB shows substantially deviated conformations and coordinates between the apo- and holo-crystal forms of the protein. The selected residues are well positioned to detect similar conformational transitions, β-strand formation (35–37) as well as the loop movement from position 81 or 78 in solution.

3.1. Circular dichroism

Far-UV CD experiments were performed to ensure that all mutants of TL have the native fold (Fig. 2). At pH 7.3, all mutant proteins, except W35C81, show similar spectra. All spectra are very close to that of the corresponding single Trp mutants as well as native TL [2]. Therefore, the additional Cys mutation at either position 81 or 78 does not generate structural perturbation. The result is consistent with the previous study [34] where position 81 was used for Cys/dansyl labeling. The far-UV CD spectrum of W35 has previously been discussed [2,24]. The minor alterations observed in this mutant were attributed to small changes in the packing of secondary structural elements. The far-UV CD spectrum of W35C81 is almost identical to that of analogous mutant W35. All single Trp mutants show similar ligand binding [27], which is considered the major function of TL. Therefore, at pH 7.3, all mutant proteins preserve the native fold and possess the ligand binding function. At pH 3.0, TL undergoes structural changes that show characteristic features of the molten globule state [35]. Consistent with that state, ANS binding to TL is enhanced significantly at low pH. CD spectra of the mutants at pH 3.0 (Fig. 2) closely resemble those previously described for single Trp mutants [34]. Interestingly, the CD spectrum of W35C81 shows a perturbation at pH 7.3 but no additional perturbation at pH 3 and is quite similar to the spectra of other mutant proteins. Therefore, it can be concluded that all mutant proteins considered in this study experience the same structural transitions at low pH and are appropriate for pH induced structural study.

As an example, the CD spectra of the W33C81 mutant at pH values of 7.3 and 3.0 were analyzed to calculate the secondary structure content (Table 1). Although the "nrmsd" values differ, all algorithms used in the calculation generated similar data. The results are consistent with previously published data for native TL [35]. Interestingly, despite the noticeable differences between the CD spectra at pH 7.3 and 3.0, the calculated contents of secondary structure elements are almost identical (Table 1). However, the ratios of intensities for the positive/negative the CD bands ($|\theta_{\pi\pi^*}|/|\theta_{n\pi^*}|$) were significantly higher for the mutant proteins at pH 7.3. This parameter shows positive correlation with the degree of twisting in β-sheets [48]. In many proteins, β-sheets exhibit a twist that lower the free energy [49] and, therefore, increase protein stability. Therefore, despite the fact that the secondary structure contents of TL at pH 7.3 and 3.0 are similar, the protein is less stable at low pH. The data support the previously published molten globule transition [33,35].

3.2. Steady-state fluorescence

The fluorescence λ_{max} values of single Trp/Cys mutants at pH 7.3 and 3.0 are shown in Fig. 3 and are very close to those of corresponding single Trp mutants studied previously [38]. The parameters of Trp

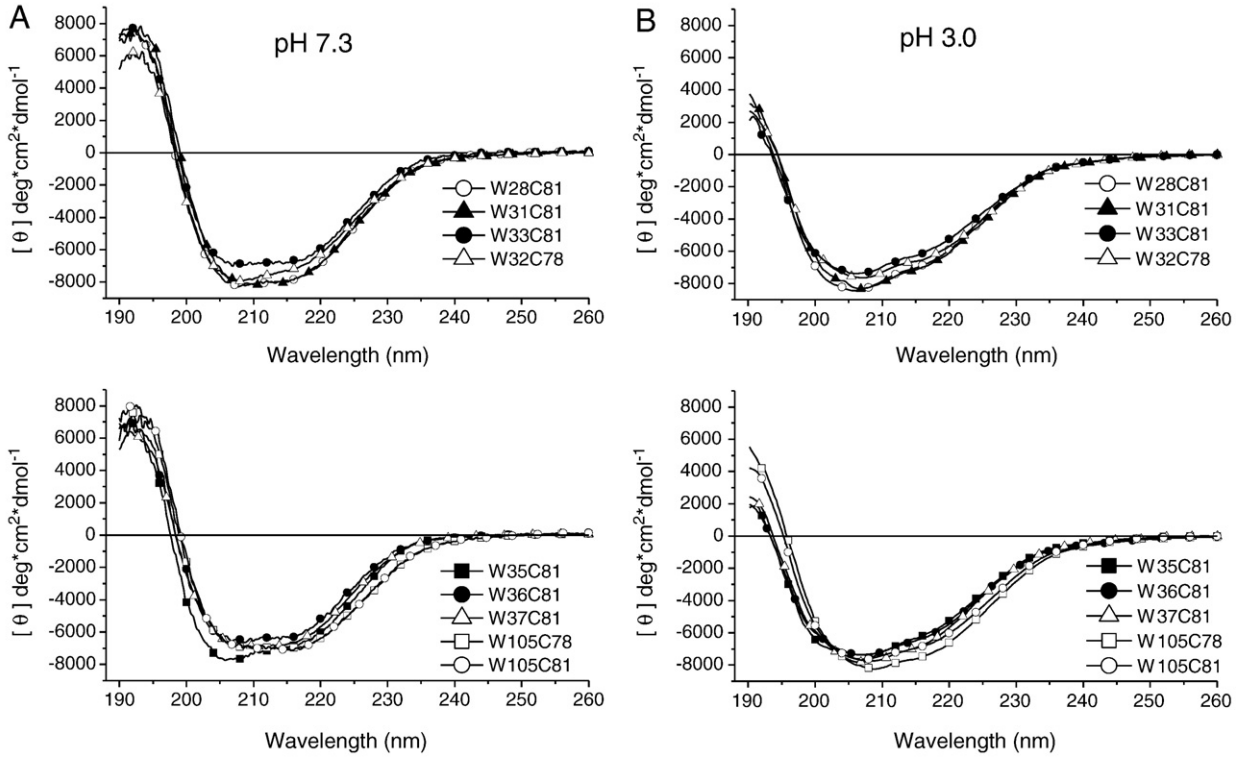

Fig. 2. Far-UV CD spectra of TL mutants considered for RET study at pH 7.3 (A) and pH 3.0 (B).

Table 1
Secondary structure content for TL (W33C81, as an example) at pH values of 7.3 and 3.0 determined from CD spectra.

Protein	Program	α-helix (%)[a]			β-strand (%)[b]			Turn	Unrd[c]	nrmsd
		$H(r)$	$H(d)$	$\sum H$	$S(r)$	$S(d)$	$\sum S$	(%)	(%)	
W33C81, pH 7.3	CONTINLL	3.6	6.2	9.8	23.7	12.0	35.7	23.3	31.1	0.033
	SELCON3	5.7	7.5	13.2	21.9	11.3	33.2	19.0	24.3	0.345
	CDSSTR	1.1	5.5	6.6	24.9	12.0	36.9	22.9	32.1	0.086
W33C81, pH 3.0	CONTINLL	3.6	6.9	10.5	21.1	12.0	33.1	22.9	33.5	0.024
	SELCON3	4.1	7.6	11.7	21.5	12.1	33.6	22.2	31.7	0.163
	CDSSTR	−0.1	5.2	5.1	23.3	12.9	36.2	24.3	33.6	0.131

[a] $H(r)$ and $H(d)$ are for regular and distorted α-helix, respectively. $\sum H = H(r) + H(d)$.
[b] $S(r)$ and $S(d)$ are for regular and distorted β-strands, respectively. $\sum S = S(r) + S(d)$.
[c] Unrd is for unordered fraction.

fluorescence, particularly fluorescence λ_{max}, are very sensitive to its environment [2,50,51]. Therefore, consistency between the fluorescence λ_{max} values in two sets of the mutants, single Trp and single Trp/Cys, is further support for the fact that additional Cys mutation does not perturb the structure of TL.

3.3. Time-resolved fluorescence

The lifetime components were analyzed to understand the changes in average lifetimes of the single Trp mutants in low pH transition (Table 2). The changes in the average lifetimes of Trp fluorescence can be due to either changes in the populations of lifetime components (population reshuffling, f_{PR}) or the fluorescence lifetimes of the components (dynamic quenching, f_{DQ}) (Fig. 4A). Population reshuffling governs the small decrease in the amplitude-averaged lifetime of Trp at position 35. This factor negates the contribution of increased fluorescence lifetimes (unquenching) in low pH transition (Fig. 4A). In contrast, the same parameter (f_{PR}) is the reason for the increased average lifetime of Trp 37 while the dynamic quenching parameter is not changed. Changes in Trp fluorescence lifetime components, which may be ascribed to distinct side chain rotamers [50,52,53], do not show any favored rotamer conformation for quenching (Fig. 4B). At low pH transition, the quenching efficiencies for the Trp residues at various positions differ from each other but the components change in tandem. The exceptions are positions 27 and 37. The fluorescence lifetime for the third component is decreased, although that for the first and second components is increased (Fig. 4B).

The quantum yields and fluorescence lifetimes of tryptophans differ significantly at various positions in the loops as well as at pH 7.3 versus pH 3.0 (Table 2). Most of the single Trp mutants at both pH values (7.3 and 3.0) show the radiative rate constants, k_r, comparable

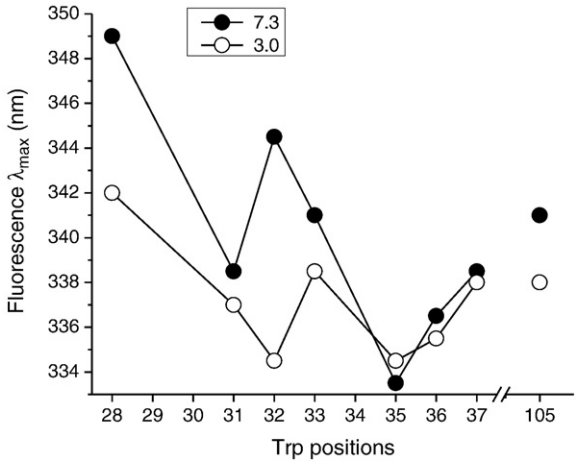

Fig. 3. λ_{max} values from the corrected fluorescence spectra of the single Trp/Cys mutants located in the loops AB and GH. Cys was invariant at position 81 in the mutants.

to that obtained for 3-methylindole, tryptophan zwitterions, and *N*-acetyltryptophanamide ($40 \div 60 \times 10^6\ s^{-1}$) [54]. This indicates that generally the decreased quantum yields and average lifetimes are the result of dynamic quenching of nearby quenching groups. However, significantly decreased k_r value (for example, $13.9 \times 10^6\ s^{-1}$ for W37C81) indicates the presence of static quenching. The reason is that static quenching decreases the quantum yield but not the fluorescence lifetime of the fluorophore. In proteins, the static quenching originates from non-fluorescent complex formation between Trp side chain in the ground state and the quencher groups. This implies that the non-fluorescent complex is formed at the time of excitation and the excited state is quenched before fluorescence occurs. In TL, position 37 is in close proximity to the –S–S– bond (between Cys61 and Cys153) [2,28,55], which is a very effective quencher [56]. Therefore, it is reasonable to speculate that the static quenching can be the result of interaction between Trp37 and –S–S– bond. It should be mentioned that very short lifetimes (<100 ps), which are below the resolution of our instrument, will be accounted as static quenching.

3.4. RET involving the loop AB and GH

Fluorescence lifetime parameters of the two sets of the mutants, Trp alone and Trp–dansyl pair, at pH 7.3 and 3.0 are shown in Table 2. In all cases, three lifetimes were necessary to describe the fluorescence intensity decays. As an example, frequency-domain intensity decay curves for the mutant W35C81, with and without the dansyl label, at pH 7.3 and 3.0 are shown in Fig. 5. The fluorescence lifetimes and RET parameters are shown in Tables 2 and 3. At pH 7.3 there are discernable differences in decay curves of the frequency-dependent phase angle and modulation measurements (with and without the dansyl label). These differences decrease significantly at pH 3.0 (Fig. 5 and Table 3). Decreased differences in $<\tau>$ values are indicative of decreased RET at pH 3.0 and, therefore, reflect increased distance between positions 35 and 81 in the low pH transition (Table 3).

Although in different degrees, amplitude-averaged lifetimes, $<\tau>$, of dansyl-labeled mutants are consistently lower than that of corresponding unlabeled mutants (Table 2). The data indicate that RET and therefore distances, vary between Trp and dansyl groups in the studied mutants. As an example the spectral overlap between the fluorescence of Trp35 and the absorbance of dansyl81 (the mutant W35Dansyl81) is shown in Fig. 6. For the dansyl-labeled mutants, the Förster distances (R_0) cover the range 20.9–15.2 Å. Disparity in the R_0 values reflects differences in quantum yield values of the corresponding Trp residues rather than the spectral overlap integrals (Table 3).

Inter-loop distances between residues from the loops AB and GH to residue 81 in the loop EF at pH 7.3 and 3.0 are summarized in Fig. 7. For comparison, the corresponding distances from the crystal structures of TL in apo- and holo-forms are also provided. The similarity of the distance distributions between two forms of TL, apo-TL in solution at pH 3.0 and holo-TL in crystal form at pH 8.0, is

Table 2
Fluorescence lifetime parameters for apo-Trp mutants (with and without dansyl label) of TL.

Trp mutant	α_1[a]	α_2	α_3	τ_1[b] (ns)	τ_2 (ns)	τ_3 (ns)	τ_{av}[c] (ns)	$\langle\tau\rangle$[d] (ns)	Q[e]	$k_r\times10^{-6}$[f] (s^{-1})	χ^2
W28C81 pH 7.3	0.41	0.35	0.24	0.43	2.58	9.02	6.79	3.24	0.13	40.1	0.8
W28Ds[g]81 pH 7.3	0.66	0.20	0.13	0.24	1.82	6.93	4.88	1.44			0.8
W28C81 pH 3.0	0.48	0.36	0.16	0.43	2.18	5.45	3.52	1.86	0.07	37.6	0.4
W28Ds81 pH 3.0	0.62	0.29	0.10	0.27	1.64	5.12	2.95	1.12			0.8
W31C81 pH 7.3	0.42	0.40	0.18	0.49	2.04	5.25	3.44	1.98	0.06	30.3	0.5
W31Ds81 pH 7.3	0.57	0.27	0.16	0.27	1.18	3.96	2.65	1.11			0.9
W31C81 pH 3.0	0.48	0.38	0.14	0.39	1.90	5.00	3.07	1.61	0.07	43.5	0.6
W31Ds81 pH 3.0	0.63	0.26	0.12	0.22	1.35	3.88	2.40	0.93			0.7
W32C78 pH 7.3	0.38	0.49	0.14	0.63	2.72	6.63	3.97	2.48	0.10	40.3	0.5
W32Ds78 pH 7.3	0.57	0.27	0.16	0.32	1.39	3.78	2.47	1.16			0.6
W32C78 pH 3.0	0.38	0.39	0.23	0.46	2.01	4.70	3.28	2.02	0.12	59.4	0.3
W32Ds78 pH 3.0	0.59	0.30	0.11	0.27	1.48	4.13	2.45	1.07			0.6
W32C81 pH 7.3	0.35	0.43	0.22	0.46	2.27	5.53	3.83	2.35	0.10	42.6	0.4
W32Ds81 pH 7.3	0.83	0.14	0.03	0.35	1.76	5.76	2.16	0.71			0.5
W32C81 pH 3.0	0.42	0.40	0.18	0.45	2.16	4.88	3.23	1.93	0.12	62.2	0.5
W32Ds81 pH 3.0	0.63	0.29	0.09	0.30	1.33	4.08	2.16	0.92			0.5
W33C81 pH 7.3	0.36	0.54	0.10	0.61	2.43	6.03	3.28	2.13	0.08	37.6	0.4
W33Ds81 pH 7.3	0.44	0.35	0.21	0.36	1.66	3.99	2.77	1.58			0.6
W33C81 pH 3.0	0.45	0.40	0.15	0.44	2.04	4.91	3.07	1.75	0.08	45.7	0.3
W33Ds81 pH 3.0	0.64	0.31	0.06	0.38	2.00	5.54	2.66	1.18			0.8
W35C81 pH 7.3	0.33	0.26	0.41	0.41	2.06	4.73	3.96	2.61	0.12	46.0	0.6
W35Ds81 pH 7.3	0.48	0.30	0.22	0.32	1.18	4.48	3.27	1.49			0.6
W35C81 pH 3.0	0.37	0.41	0.22	0.45	2.42	5.66	3.94	2.39	0.13	54.4	0.3
W35Ds81 pH 3.0	0.43	0.27	0.30	0.34	1.80	4.35	3.41	1.94			0.5
W36C81 pH 7.3	0.29	0.52	0.19	0.58	2.62	5.52	3.68	2.59	0.13	50.2	0.4
W36Ds81 pH 7.3	0.66	0.23	0.10	0.41	1.92	5.12	2.92	1.24			0.8
W36C81 pH 3.0	0.38	0.38	0.24	0.46	1.92	4.14	2.96	1.91	0.11	57.6	0.4
W36Ds81 pH 3.0	0.76	0.16	0.07	0.22	1.28	3.82	2.06	0.65			0.4
W37C81 pH 7.3	0.59	0.29	0.12	0.37	1.89	5.65	3.43	1.44	0.02	13.9	0.7
W37Ds81 pH 7.3	0.76	0.17	0.07	0.25	1.58	4.83	2.64	0.80			0.7
W37C81 pH 3.0	0.48	0.32	0.19	0.39	2.05	5.25	3.62	1.86	0.07	37.6	0.4
W37Ds81 pH 3.0	0.61	0.25	0.13	0.25	1.60	4.70	3.05	1.18			0.5
W105C78 pH 7.3	0.55	0.35	0.10	0.48	2.08	5.67	3.11	1.57	0.05	31.8	0.5
W105Ds78 pH 7.3	0.68	0.26	0.06	0.41	1.60	4.63	2.14	0.98			0.6
W105C78 pH 3.0	0.57	0.33	0.10	0.34	1.55	4.47	2.48	1.15	0.05	43.5	0.5
W105Ds78 pH 3.0	0.78	0.17	0.05	0.28	1.26	3.57	1.58	0.61			0.4
W105C81 pH 7.3	0.58	0.31	0.11	0.48	2.03	5.62	3.20	1.53	0.04	26.1	0.6
W105Ds81 pH 7.3	0.67	0.24	0.09	0.23	1.63	5.41	3.20	1.03			0.7
W105C81 pH 3.0	0.55	0.34	0.11	0.36	1.53	4.64	2.63	1.23	0.04	32.5	0.5
W105Ds81 pH 3.0	0.56	0.29	0.15	0.27	0.86	2.86	1.79	0.83			0.8

[a] Normalized preexponential factor.
[b] Decay time.
[c] Intensity averaged lifetime.
[d] Amplitude averaged lifetime.
[e] Quantum yield.
[f] Radiative rate constant.
[g] Dansyl.

remarkable. Disparities in factual values can partly be attributed to differences in the methods of the measurements. In this study, RET measurement assigns center-to-center distance between the indole group of Trp and dansyl label. However, distances between corresponding residues from the crystal structures are taken using C^{α} atoms of the residues. The difference between the two methods will be maximal when side chains of the residues, located in opposing sites, point away from each other. To check the accuracy of distance measurements, the reference point labeled with dansyl at position 81 in W32Ds81, was changed to 78 (W32Ds78). The side chain of residue 78 points away from the opposing loop AB (Table 3 and Fig. 1). Accordingly, the use of RET in the respective mutants, the distance from the position 78 should be expected to be somewhat greater compared to that of the position 81. Indeed, distance measurements corroborate that expectation (Table 3). However, switching the reference point from positions 81 to 78 would minimally affect distances if applied to the neighboring loops, EF and GH (Fig. 1). Indeed, at pH 7.3 distance measurements for the mutants W105Ds81 and W105Ds78 are practically identical (Table 3).

The measured distances for the residues 35–37 in loop AB at pH 3.0 reflect the periodicity of a β-strand (Figs. 1 and 7), which recapitulates the crystal structure of TL in holo-form [28]. However, the distance distribution for apo-TL in crystal (pH 8.0) form is different from that in solution (pH 7.3). Surprisingly, these distance distribution patterns appear as the mirror image of each other. Although Trp105 shows distinct conformational change at low pH, its distance from reference point, position 81, at pH 3.0 does not differ from that measured at pH 7.3.

The fluorescence lifetime as well as RET parameters for holo-TL mutants at pH values of 3.0 and 7.3 are shown in Tables 4 and 5, respectively. At pH 3.0, the loop AB in holo-TL is minimally altered (RMS = 0.9 Å) compared to that in apo-TL (Fig. 8A). The loop conformation has the same pattern. β-strand periodicity of the residues 35–37 is more pronounced in holo-TL. However, the position 105 of the loop GH shows considerable movement, about 4.3 Å. In contrast to pH 3.0, the loop AB residues are significantly closer to position 81 (RMS = 3.1 Å) at pH 7.3. The position 105 moves about 3.1 Å with ligand binding at pH 7.3, similar to that observed at pH 3.0.

4. Discussion

The loops at the open end of the barrel of TL, predominantly the loop AB, are implicated in ligand binding [27,28,38]. Significant shifts observed for the fluorescence λ_{max} values (Fig. 3) in the low pH

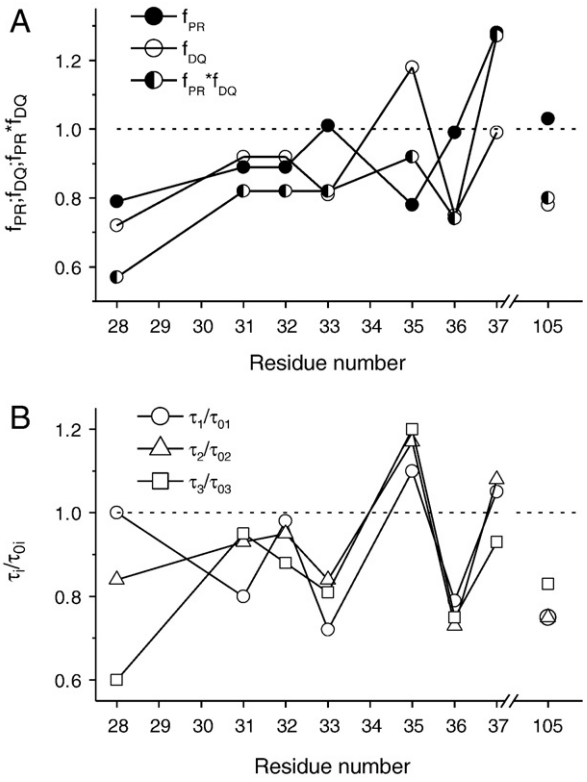

Fig. 4. Fluorescence lifetime parameter of single Trp mutants of TL in the transition from pH 7.3 to 3.0. (A) The resolution of fluorescence lifetime changes ($\frac{\langle\tau\rangle}{\langle\tau_0\rangle} = f_{PR} \times f_{DQ}$) into the components (population reshuffling (f_{PR}), and dynamic quenching (f_{DQ}) parameters). (B) Changes in fluorescence lifetime component. The components of the fluorescence lifetime of Trp are grouped as $\tau_1 = 0.22–0.63$ ns, $\tau_2 = 0.86–2.72$ ns and $\tau_3 = 2.86–9.02$ ns. The parameters were calculated only for the mutants where Cys was invariant at position 81.

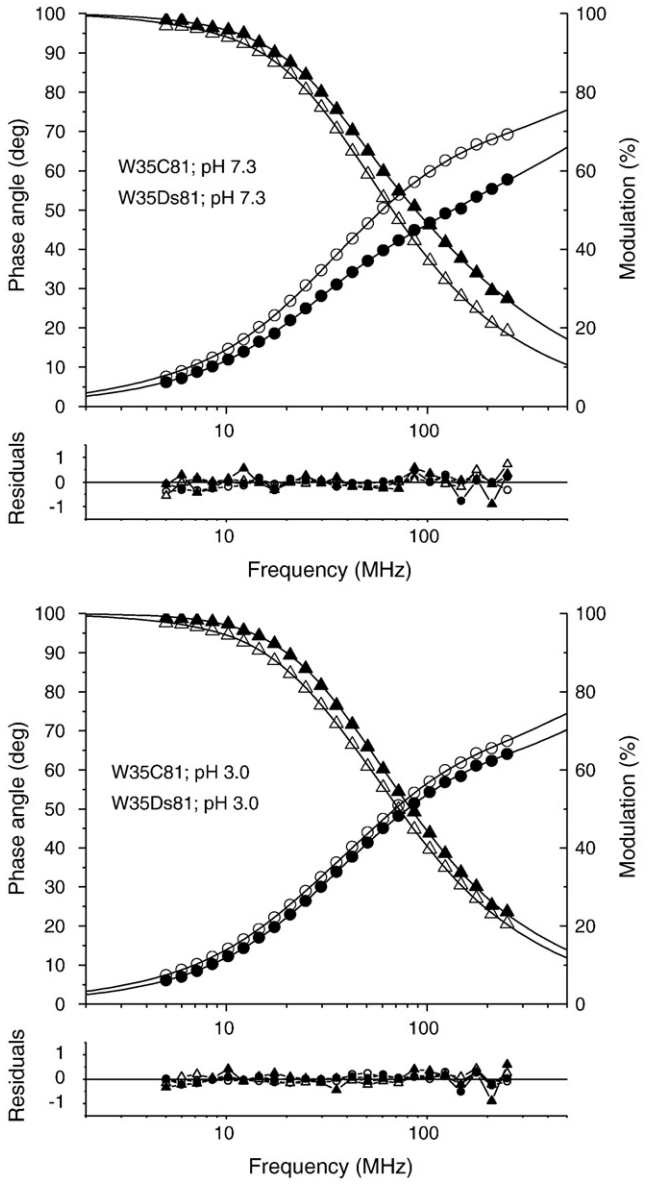

Fig. 5. Phase angle (circles) and modulation (triangles) data for the fluorescence intensity decays of TL mutant W35C81, dansyl-labeled Cys81 (solid symbols), and unlabeled Cys81 (open symbols) for detection of RET at pH 7.3 and 3.0. Lines represent the best triple-exponential fit for the parameters given in Table 2.

transition indicate substantial changes in the environments of Trp side chains. This effect has been shown previously to reflect the combination of various processes [38]. Reduction of pH alters the protonation state of titratable side chains. Positive or negative charges in different positions around the indole ring of Trp can produce both blue and red shifts of fluorescence λ_{max} [51]. Conformational changes induced by the low pH transition reshuffle the accessibilities of the residues of the loop AB to solvent [38]. The increased and decreased solvent accessibility produce respective red and blue shifts in Trp fluorescence λ_{max} [45]. Analysis of Trp fluorescence lifetime components in low pH transition identifies the significant rotamer population reshuffling for the residues 27, 35, and 37 (Fig. 4). Since the rotamer population of the Trp side chain depends on backbone conformation, the result shows significant conformational transitions for these residues. Amplitude-averaged lifetimes as well as lifetime components of Trp fluorescence mostly decreased in the low pH transition, except for position 35. The result is consistent with quenching properties of certain amino acids (Glu, Asp and His), which are effective quenchers only in protonated states [56]. Therefore, decreased fluorescence lifetimes can generally be expected in low pH transitions.

Two independent studies [28,38] concur that the electrostatic interaction between residues Glu27 (loop AB) and Lys108 (loop GH) regulates the conformation of the loop AB for ligand binding. In one of these studies, a tryptophan substitution at position 28 was chosen to probe the nearest electrostatic potential. pH titration curves of fluorescence λ_{max} of Trp28 differ significantly in apo- versus holo-TL [38], but differences are not apparent for Trp substitution in other positions. In addition mutation of either residue Glu27 or Lys108 significantly alters ligand binding [27]. Together, these data indicate that ligand binding stabilizes the conformations of the loops that embrace the electrostatic interaction between Glu27 and Lys108. Therefore, pH induced conformational changes are functionally significant for ligand binding. In accord with these findings, the distance between residues 28 and 81 is increased at pH 3; the side chain of Glu27 is protonated, compared to that measured at pH 7.3 (Table 3 and Fig. 7C).

The movement of the loops EF and GH in the apo-holo transition of TL in crystal form (pH 7.9–8.0) was described [28] as similar to that in solution of the low pH transition [34]. The new fact that the loop AB conformation of apo-TL in solution at low pH resembles very closely that of holo-TL in the crystal form at pH 8.0 may have significant implications. Apo-TL may sample the "holo-like" conformations (conformations similar to that of ligand–TL complex) (Fig. 7A), which can be considered as excited protein states for ligand binding. Therefore, ligand binding could increase the population of the preexisting "holo-like" conformations, a prerequisite for a binding mechanism through conformational selection.

Table 3
RET parameter and distance data for Trp–dansyl pairs in apo-proteins.

Trp mutant	⟨τ⟩[a] (ns)	E[b]	f_a[c]	E_{corr}[d]	J*10^{-13} M^{-1} cm^{-1}[e] (nm)^4	R_0[f] (Å)	R[g] (Å)
W28C81, pH 7.3	3.24						
W28Ds[h]81, pH 7.3	1.44	0.56	0.64	0.88	3.92	20.7	14.9
W28C81, pH 3.0	1.86						
W28Ds81, pH 3.0	1.12	0.40	0.64	0.63	4.26	18.7	17.1
W31C81, pH 7.3	1.98						
W31Ds81, pH 7.3	1.11	0.44	0.73	0.60	4.05	18.3	17.1
W31C81, pH 3.0	1.61						
W31Ds81, pH 3.0	0.93	0.42	0.73	0.58	4.27	18.8	17.8
W32C78, pH 7.3	2.48						
W32Ds78, pH 7.3	1.16	0.53	1.22	0.53	3.68	19.6	19.2
W32C78, pH 3.0	2.02						
W32Ds78, pH 3.0	1.07	0.47	1.22	0.47	4.28	20.6	21.0
W32C81, pH 7.3	2.35						
W32Ds81, pH 7.3	0.71	0.70	1.04	0.70	3.68	19.6	17.0
W32C81, pH 3.0	1.93						
W32Ds81, pH 3.0	0.92	0.52	1.04	0.52	4.28	20.6	20.3
W33C81, pH 7.3	2.13						
W33Ds81, pH 7.3	1.58	0.26	0.86	0.30	3.96	19.1	22.0
W33C81, pH 3.0	1.75						
W33Ds81, pH 3.0	1.18	0.33	0.86	0.38	4.29	19.3	20.9
W35C81, pH 7.3	2.61						
W35Ds81, pH 7.3	1.49	0.43	0.69	0.62	4.12	20.6	19.0
W35C81, pH 3.0	2.39						
W35Ds81, pH 3.0	1.94	0.19	0.69	0.28	4.33	20.9	24.4
W36C81, pH 7.3	2.59						
W36Ds81, pH 7.3	1.24	0.52	0.98	0.53	4.14	20.9	20.5
W36C81, pH 3.0	1.91						
W36Ds81, pH 3.0	0.65	0.66	0.98	0.67	4.34	20.4	18.1
W37C81, pH 7.3	1.44						
W37Ds81, pH 7.3	0.80	0.44	0.88	0.50	4.02	15.2	15.2
W37C81, pH 3.0	1.86						
W37Ds81, pH 3.0	1.18	0.37	0.88	0.42	4.34	18.8	19.8
W105C78, pH 7.3	1.57						
W105Ds78, pH 7.3	0.98	0.38	1.17	0.38	3.77	17.5	19.0
W105C78, pH 3.0	1.15						
W105Ds78, pH 3.0	0.61	0.47	1.17	0.47	4.27	17.6	18.0
W105C81, pH 7.3	1.53						
W105Ds81, pH 7.3	1.03	0.33	1.05	0.33	4.09	17.1	19.2
W105C81, pH 3.0	1.23						
W105Ds81, pH 3.0	0.83	0.33	1.05	0.33	4.09	17.1	19.2

[a] Amplitude averaged lifetime.
[b] The efficiency of resonance energy transfer.
[c] A fraction of dansyl labeling.
[d] The efficiency of resonance energy transfer corrected for incomplete labeling.
[e] The overlap integral.
[f] The Förster distance (distance at which 50% energy transfer occurs).
[g] Donor–acceptor distance.
[h] Dansyl.

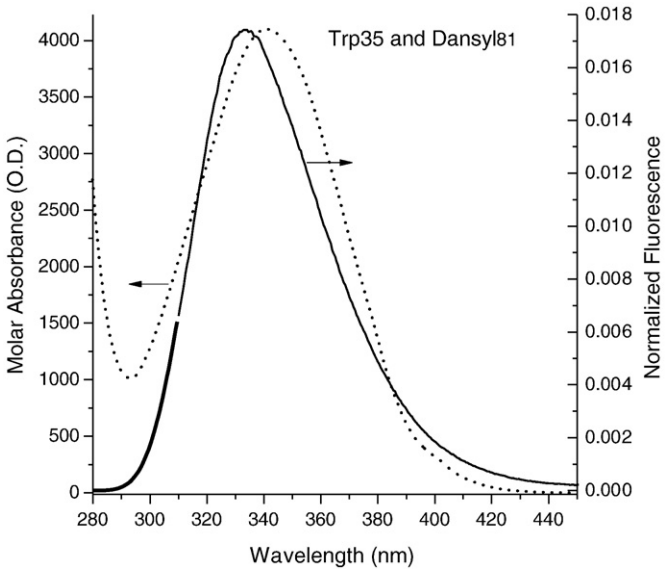

Fig. 6. The absorption (left) and emission (right) spectra for the dansyl-labeled mutant, Trp35Ds81. The blue side of the emission spectra (bold solid lines) was constructed using the log-normal function (see Materials and methods).

Saturation of apo-TL with palmitic acid (1:2) minimally alters the loop AB conformation (RMS = 0.9 Å) (Fig. 8A). However, the position 105 of the loop GH shows the displacement of about 4.5 Å. The result is consistent with previously reported ligand binding studies of TL. At low pH, TL shows significantly decreased ligand affinity to the palmitic acid analog, 16-AP (16-(9-anthroyloxy)palmitic acid) [34]. Therefore, this conformation can be classified as a "low-affinity" binding mode. Interestingly, the crystal structure of holo-TL describes binding of the artificial ligand 1,4-butanediol, for which Tyr/Trp fluorescence titration experiment did not show any sign of binding [28]. The presence of this ligand in the crystal structure has been rationalized by its high concentration in the crystallization solution. The current results performed in solution suggest that the conformation of the loop AB at pH 3.0, which is very similar to that of the crystal structure of the holo-TL at pH 8, represents "low-affinity" excited state of the protein.

The transition from pH 3.0 to 7.3 generates "crankshaft"-like motion in the loop AB that sets "high-affinity" binding mode (K_d = 0.8 μM for 16-AP [34]). The decreased distances indicate that the loop AB has more compact conformation (RMS = 3.1 Å) in the "high-affinity" excited protein state (Fig. 8B). Perhaps, this conformation increases contact sites between the ligand and the side chains. Indeed, C12SL, the spin labeled analog of palmitic acid, shows numerous contact sites for the loop AB [27]. In accord with previous studies [28,38], data reveal that protonation state of Glu 27 modulates the loop AB conformations for low- and high-affinity binding modes. In holo-TL at pH 7.3, distance between positions 28 and 81 is further decreased to about 10.4 Å from 14.9 Å (Fig. 8B). No such movement is detected at low pH in the "low-affinity" mode, where Glu27 is protonated (Fig. 8A). Data suggest that in holo-TL at pH 7.3 the distance between Glu27 and Lys108 is decreased. As a result, electrostatic interaction between these residues will be enhanced.

Previous ligand binding studies for TL have exhibited the features of both binding mechanisms termed as the "induced fit" (binding first) [22,28,35] and "conformational selection" (conformational selection first) [27]. Evidence for induced fit originates from circular dichroism experiments. Ligand binding to TL results in an increased amount of β-sheet structure [35]. The crystal structure analysis of holo-TL confirmed this finding. In crystal forms, holo-TL has ~20% higher β-sheet content compared to that of apo-TL [28]. Additional evidence for an induced fit mechanism comes from studies in solution. Ligand binding generates conformational changes of the residues located in the FG and GH loops [22,27]. In addition crystallography studies show that conformational changes for intracavitary residues, Met39 and Phe99, facilitate ligand binding [28]. Such structural rearrangements as well as conformational changes that facilitate ligand binding [22,28,35] are characteristic for an induced fit mechanism. The evidence for conformational selection is rooted in the observation of excited protein states, which are selected by ligand binding [27]. In addition, the crystal structure of TL in holo-form [28] and distance measurements performed in this study do not suggest a "lid-over" conformation for the loop AB. The results very much favor the "conformational selection" mechanism for ligand binding. Lately, conformational selection, the more recently introduced mechanism, has attracted enormous attention [57–61]. One of the most attractive features of this mechanism is that it relies on the energy landscape model of protein dynamics [62]. It is widely accepted that apo-forms of proteins do not have one unique conformation. Rather a large number of conformations are populated according to their energy. The higher energy conformations (excited protein states) are sparsely populated and active for ligand binding. Therefore, a binding event by

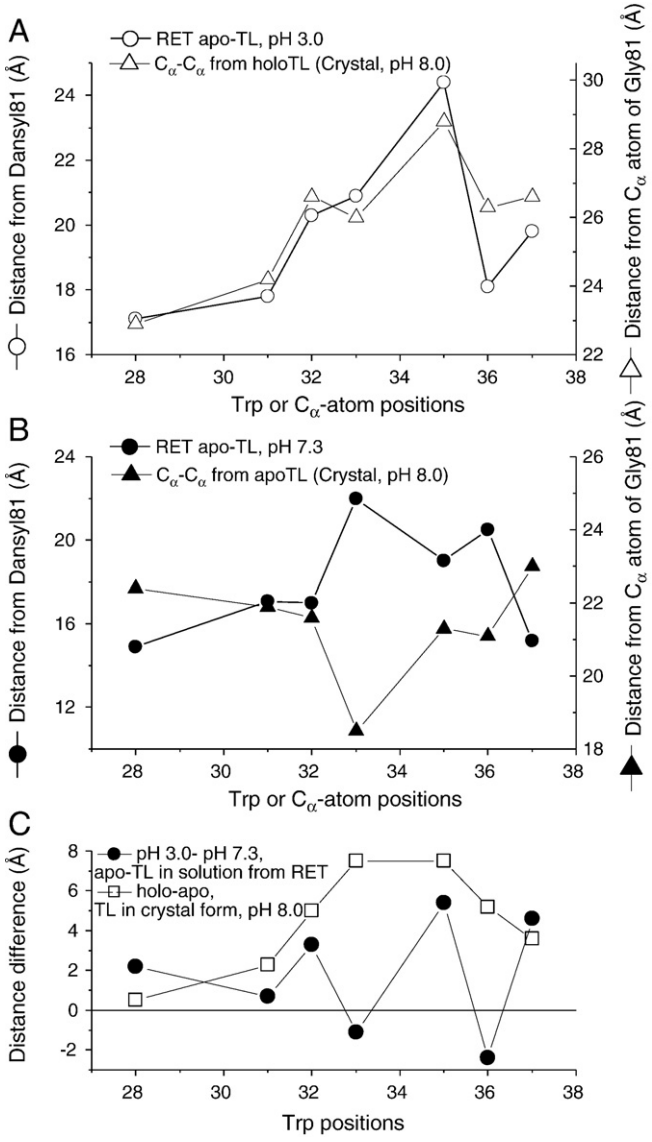

Fig. 7. Comparison of the measured inter-loop distances from RET to that of the crystal structure of TL. (A) RET data for apo-TL at pH 3.0 is similar to that of the crystal structure for holo-TL at pH 7.3; (B) the shape of the RET data in solution for apo-TL at pH 7.3 appears to form a mirror image of the data obtained from crystal structure of TL at pH 8.0; (C) Low pH induced changes in distances between residues of the loop AB and the residue 81 of the loop EF. For comparison with TL in crystal forms, changes in distances (C^{α}–C^{α}) between the same residues in apo-holo transition are also included.

this mechanism selects excited protein states and shifts the population toward those states. In TL, bound fatty acid does not have a unique position, but is distributed asymmetrically within binding cavity yielding the binding energy landscape [27]. The findings indicate that binding selects not unique but multiple "excited protein states" for ligand binding.

Compared to other members of lipocalin family, TL exhibits promiscuous ligand binding. The binding to ligands, which significantly differ in size and shape, requires high structural dynamism. The motion of the loop AB observed in this (Figs. 7 and 8) and another study [28] suggests that the loop can potentially adopt various conformations to match the size and/or shape of an assortment of ligands. In contrast, the crystal structures of porcine odorant binding protein (pOBP), which bind to various classes of ligands, are practically identical (RMS = 0.3 Å for 295 atoms) for holo- and apo-forms [63]. However, another closely related lipocalin, β-lactoglobulin, shows relatively smaller structural and conformational rearrangements in ligand binding that appear localized to the loop EF [64]. The pH-dependent changes modulate "open" and "closed" conformations of the loop EF. This loop movement is functional and regulates ligand binding in β-lactoglobulin [65]. Interestingly, molecular dynamics simulations performed on β-lactoglobulin in "open" and "closed" conformations suggest the presence of free energy gradients originated by fluctuations of the structure [37]. Structural changes observed from the palmitic acid binding experiments are very similar to those of pH titration in NMR experiments [64]. The binding mechanism for β-lactoglobulin has been interpreted as a population shift scheme, i.e., shift to "open" conformation from preexisting "open" and "closed" conformations. However, unlike TL, the loop AB of β-lactoglobulin contributes to dimer formation and has not been implicated in ligand binding.

As mentioned above, ligand binding by TL, along with conformational selection, also shows the distinct features of the induced fit mechanism. Because they are closely connected, it is not surprising to have the features of both mechanisms for the same protein. It has been pointed out that the ligand binding mechanism can depend on (or can be switched by) both the ligand and protein concentrations [58]. Moreover, theoretical calculations reveal that an induced fit binding mechanism is applicable only if interacting species display preexisting complementarity [66]. The conformational rearrangements after initial conformational selection are apparently very important for optimization of ligand binding as well as for selective recognition by a receptor. Otherwise, the receptor could be saturated

Table 4
Fluorescence lifetime parameters for RET in holo-TL at pH 3.0.

Trp mutant	⟨τ⟩[a] (ns)	E	f	E_{corr}	R_0 (Å)	R (Å)
Holo-W28C81	1.84					
Holo-W28Ds81	1.15	0.38	0.64	0.59	18.6	17.5
Holo-W31C81	1.63					
Holo-W31Ds81	1.01	0.38	0.73	0.52	18.9	18.6
Holo-W32C81	2.02					
Holo-W32Ds81	0.93	0.54			20.3	19.8
Holo-W33C81	1.72					
Holo-W33Ds81	1.22	0.30	0.86	0.35	19.7	21.8
Holo-W35C81	2.43					
Holo-W35Ds81	2.09	0.14	0.69	0.20	20.7	26.1
Holo-W36C81	1.82					
Holo-W36Ds81	0.49	0.73.	0.98	0.74	20.0	16.8
Holo-W37C81	1.94					
Holo-W37Ds81	1.22	0.37	0.88	0.42	19.0	20.1
Holo-W105C81	1.22					
Holo-W105Ds81	0.39	0.68	1.0	0.68	17.6	15.5

[a] All symbols are the same as in Table 3.

Table 5
Fluorescence lifetime parameters for RET in holo-TL at pH 7.3.

Trp mutant	⟨τ⟩[a] (ns)	E	f	E_{corr}	R_0 (Å)	R (Å)
Holo-W28C81	3.11					
Holo-W28Ds81	1.14	0.63	0.64	0.98	19.8	10.4
Holo-W31C81	1.69					
Holo-W31Ds81	0.61	0.64	0.73	0.88	18.3	13.1
Holo-W32C81	2.14					
Holo-W32Ds81	0.74	0.65	1.04	0.65	18.9	17.0
Holo-W33C81	1.91					
Holo-W33Ds81	0.93	0.51	0.86	0.59	19.1	18.0
Holo-W35C81	2.58					
Holo-W35Ds81	1.22	0.53	0.69	0.77	20.2	16.5
Holo-W36C81	2.39					
Holo-W36Ds81	0.90	0.62	0.98	0.63	20.3	18.6
Holo-W37C81	1.26					
Holo-W37Ds81	0.46	0.63	0.88	0.72	15.2	13.0
Holo-W105C81	1.26					
Holo-W105Ds81	0.61	0.52	1.0	0.52	16.3	16.1

[a] All symbols are the same as in Table 3.

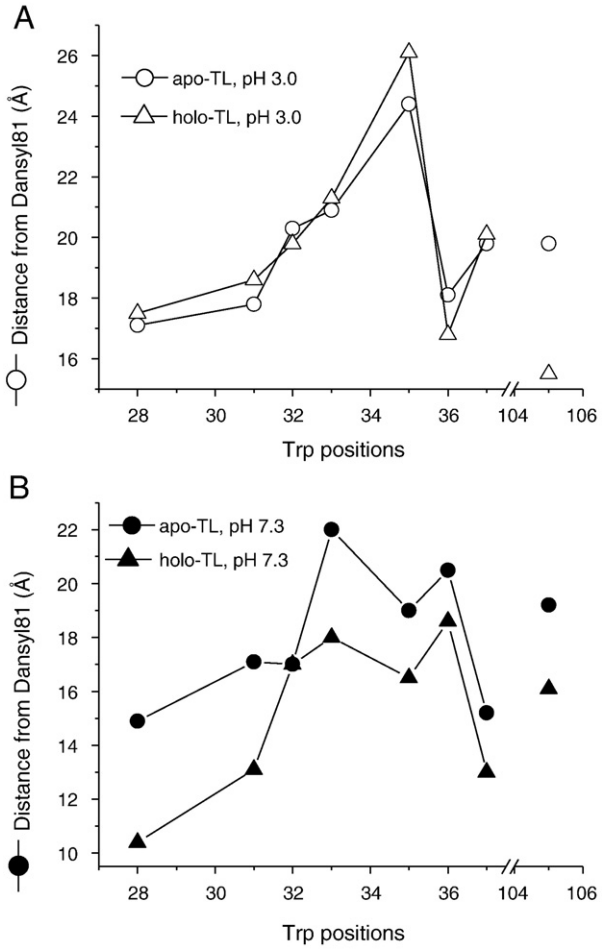

Fig. 8. Deviations of the inter-loop distances in apo-holo transition from RET measurements. (A) Measured distances for apo- and holo-TL at pH 3.0. (B) Measured distances for apo- and holo-TL at pH 7.3.

with apo-proteins in excited protein states. Therefore, a combination of both mechanisms, conformational selection and induced fit, best characterizes ligand–proteins interaction of TL as suggested for other proteins [57].

Switching the reference point (from 81 to 78) in distance measurements using mutants W32C81 and W32C78 produced the result that is consistent with their relative positions in both solution and crystal structures of TL. Therefore, it may be concluded that RET measurements are fairly accurate. However, at pH 7.3 the distance distribution patterns, therefore, conformations, for the loop AB in apo-TL in solution are different from the crystal (pH 8.0) form (Fig. 7B). They appear to resemble mirror images of each other. The result is surprising because detailed comparison of the crystal and solution structures for apo-TL have revealed excellent agreement [3]. The discrepancy cannot be rationalized by error in RET or differences in distance measurement methods. In contrast to holo-TL, the part of the loop AB, residues 25–31, is not resolved in the crystal structure of apo-TL [3]. This is indicative of conformational diversity. Therefore, it is reasonable to expect different conformations in distinct environmental conditions such as in solution at 295 K and crystal at 100 K. RET measures distances between the centers of indole and dansyl groups, compared to the C^{α}–C^{α} distance in the crystal forms of the protein. The expected difference in distance measurements is less for the crystal form than what is measured in solution between the side chains. The low pH transition generates a "crankshaft" like movement for the loop AB (Fig. 7C). If one accounts for these differences for positions 35–37, with β strand formation (Fig. 7A) one would expect even smaller movement for C^{α} atoms in solution for this transition (Fig. 7C). Surprisingly, often proteins in solution rather than in crystal form show large scale motions.

Conformational diversity of the functional regions of the protein is necessary for multi-specificity as is seen in TL. The loop AB, as the largest loop and with the greatest dynamic excursion is particularly well suited to mediate various functions.

Our understanding of protein functions is evolving. No longer are proteins considered to have absolute functional specificity with one unique structure as this would inhibit their ability to evolve new structures and functions [59]. Interestingly, the lipocalin fold functions in bacteria, plants, vertebrates and invertebrates. It has been pointed out that active site flexibility mediates promiscuity, perhaps, both structurally and functionally. For the lipocalin family, the loops at the open end of the barrel are functional determinants. For TL, the loop AB shows the ability to adopt various conformations, is fundamental to regulating the various functions.

Acknowledgments

This work was supported by the U.S. Public Health Service Grants NIH EY11224 and EY00331 as well as the Edith and Lew Wasserman Endowed Professorship in Ophthalmology (B.G.).

References

[1] D.R. Flower, The lipocalin protein family: structure and function, Biochem. J. 318 (Pt 1) (1996) 1–14.
[2] O.K. Gasymov, A.R. Abduragimov, T.N. Yusifov, B.J. Glasgow, Site-directed tryptophan fluorescence reveals the solution structure of tear lipocalin: evidence for features that confer promiscuity in ligand binding, Biochemistry 40 (2001) 14754–14762.
[3] D.A. Breustedt, I.P. Korndorfer, B. Redl, A. Skerra, The 1.8-A crystal structure of human tear lipocalin reveals an extended branched cavity with capacity for multiple ligands, J. Biol. Chem. 280 (2005) 484–493.
[4] B.J. Glasgow, A.R. Abduragimov, Z.T. Farahbakhsh, K.F. Faull, W.L. Hubbell, Tear lipocalins bind a broad array of lipid ligands, Curr. Eye Res. 14 (1995) 363–372.
[5] O.K. Gasymov, A.R. Abduragimov, E.O. Gasimov, T.N. Yusifov, A.N. Dooley, B.J. Glasgow, Tear lipocalin: potential for selective delivery of rifampin, Biochim. Biophys. Acta 1688 (2004) 102–111.
[6] O.K. Gasymov, A.R. Abduragimov, P. Prasher, T.N. Yusifov, B.J. Glasgow, Tear lipocalin: evidence for a scavenging function to remove lipids from the human corneal surface, Invest. Ophthalmol. Vis. Sci. 46 (2005) 3589–3596.
[7] O.K. Gasymov, A.R. Abduragimov, T.N. Yusifov, B.J. Glasgow, Binding studies of tear lipocalin: the role of the conserved tryptophan in maintaining structure, stability and ligand affinity, Biochim. Biophys. Acta 1433 (1999) 307–320.
[8] B.J. Glasgow, G. Marshall, O.K. Gasymov, A.R. Abduragimov, T.N. Yusifov, C.M. Knobler, Tear lipocalins: potential lipid scavengers for the corneal surface, Invest. Ophthalmol. Vis. Sci. 40 (1999) 3100–3107.
[9] B.J. Glasgow, O.K. Gasymov, A.R. Abduragimov, J.J. Engle, R.C. Casey, Tear lipocalin captures exogenous lipid from abnormal corneal surfaces, Invest. Ophthalmol. Vis. Sci. (2009).
[10] M.E. Selsted, R.J. Martinez, Isolation and purification of bactericides from human tears, Exp. Eye Res. 34 (1982) 305–318.
[11] M. Fluckinger, H. Haas, P. Merschak, B.J. Glasgow, B. Redl, Human tear lipocalin exhibits antimicrobial activity by scavenging microbial siderophores, Antimicrob. Agents Chemother. 48 (2004) 3367–3372.
[12] W. van't Hof, M.F. Blankenvoorde, E.C. Veerman, A.V. Amerongen, The salivary lipocalin von Ebner's gland protein is a cysteine proteinase inhibitor, J. Biol. Chem. 272 (1997) 1837–1841.
[13] M. Blaker, K. Kock, C. Ahlers, F. Buck, H. Schmale, Molecular cloning of human von Ebner's gland protein, a member of the lipocalin superfamily highly expressed in lingual salivary glands, Biochim. Biophys. Acta 1172 (1993) 131–137.
[14] B. Redl, P. Holzfeind, F. Lottspeich, cDNA cloning and sequencing reveals human tear prealbumin to be a member of the lipophilic-ligand carrier protein superfamily, J. Biol. Chem. 267 (1992) 20282–20287.
[15] M. Lechner, P. Wojnar, B. Redl, Human tear lipocalin acts as an oxidative-stress-induced scavenger of potentially harmful lipid peroxidation products in a cell culture system, Biochem. J. 356 (2001) 129–135.
[16] B.J. Glasgow, A.R. Abduragimov, O.K. Gassymov, T.N. Yusifov, E.C. Ruth, K.F. Faull, Vitamin E associated with the lipocalin fraction of human tears, Adv. Exp. Med. Biol. 506 (2002) 567–572.
[17] T.N. Yusifov, A.R. Abduragimov, O.K. Gasymov, B.J. Glasgow, Endonuclease activity in lipocalins, Biochem. J. 347 (Pt 3) (2000) 815–819.
[18] T.N. Yusifov, A.R. Abduragimov, K. Narsinh, O.K. Gasymov, B.J. Glasgow, Tear lipocalin is the major endonuclease in tears, Mol. Vis. 14 (2008) 180–188.
[19] A. Skerra, Anticalins as alternative binding proteins for therapeutic use, Curr. Opin. Mol. Ther. 9 (2007) 336–344.

[20] A. Skerra, Lipocalins as a scaffold, Biochim. Biophys. Acta 1482 (2000) 337–350.
[21] S. Schlehuber, A. Skerra, Duocalins: engineered ligand-binding proteins with dual specificity derived from the lipocalin fold, Biol. Chem. 382 (2001) 1335–1342.
[22] O.K. Gasymov, A.R. Abduragimov, T.N. Yusifov, B.J. Glasgow, Resolution of ligand positions by site-directed tryptophan fluorescence in tear lipocalin, Protein Sci. 9 (2000) 325–331.
[23] B.J. Glasgow, O.K. Gasymov, A.R. Abduragimov, T.N. Yusifov, C. Altenbach, W.L. Hubbell, Side chain mobility and ligand interactions of the G strand of tear lipocalins by site-directed spin labeling, Biochemistry 38 (1999) 13707–13716.
[24] O.K. Gasymov, A.R. Abduragimov, B.J. Glasgow, Ligand binding site of tear lipocalin: contribution of a trigonal cluster of charged residues probed by 8-anilino-1-naphthalenesulfonic acid, Biochemistry 47 (2008) 1414–1424.
[25] T.J. Millar, P. Mudgil, I.A. Butovich, C.K. Palaniappan, Adsorption of human tear lipocalin to human meibomian lipid films, Invest. Ophthalmol. Vis. Sci. 50 (2009) 140–151.
[26] P. Mudgil, T.J. Millar, Adsorption of apo- and holo-tear lipocalin to a bovine Meibomian lipid film, Exp. Eye Res. 86 (2008) 622–628.
[27] O.K. Gasymov, A.R. Abduragimov, B.J. Glasgow, Intracavitary ligand distribution in tear lipocalin by site-directed tryptophan fluorescence, Biochemistry 48 (2009) 7219–7228.
[28] D.A. Breustedt, L. Chatwell, A. Skerra, A new crystal form of human tear lipocalin reveals high flexibility in the loop region and induced fit in the ligand cavity, Acta. Crystallogr. D Biol. Crystallogr. 65 (2009) 1118–1125.
[29] V. Calderone, R. Berni, G. Zanotti, High-resolution structures of retinol-binding protein in complex with retinol: pH-induced protein structural changes in the crystal state, J. Mol. Biol. 329 (2003) 841–850.
[30] M.E. Newcomer, D.E. Ong, Plasma retinol binding protein: structure and function of the prototypic lipocalin, Biochim. Biophys. Acta 1482 (2000) 57–64.
[31] S.A. Roberts, A. Weichsel, Y. Qiu, J.A. Shelnutt, F.A. Walker, W.R. Montfort, Ligand-induced heme ruffling and bent no geometry in ultra-high-resolution structures of nitrophorin 4, Biochemistry 40 (2001) 11327–11337.
[32] P.M. Hwang, W.Y. Choy, E.I. Lo, L. Chen, J.D. Forman-Kay, C.R. Raetz, G.G. Prive, R.E. Bishop, L.E. Kay, Solution structure and dynamics of the outer membrane enzyme PagP by NMR, Proc. Natl. Acad. Sci. U. S. A. 99 (2002) 13560–13565.
[33] O.K. Gasymov, A.R. Abduragimov, B.J. Glasgow, Molten globule state of tear lipocalin: ANS binding restores tertiary interactions, Biochem. Biophys. Res. Commun. 357 (2007) 499–504.
[34] O.K. Gasymov, A.R. Abduragimov, T.N. Yusifov, B.J. Glasgow, Interstrand loops CD and EF act as pH-dependent gates to regulate fatty acid ligand binding in tear lipocalin, Biochemistry 43 (2004) 12894–12904.
[35] O.K. Gasymov, A.R. Abduragimov, T.N. Yusifov, B.J. Glasgow, Structural changes in human tear lipocalins associated with lipid binding, Biochim. Biophys. Acta 1386 (1998) 145–156.
[36] M. Prats, J. Teissie, J.F. Tocanne, Nature 322 (1986) 756–758.
[37] F. Fogolari, E. Moroni, M. Wojciechowski, M. Baginski, L. Ragona, H. Molinari, MM/PBSA analysis of molecular dynamics simulations of bovine beta-lactoglobulin: free energy gradients in conformational transitions? Proteins 59 (2005) 91–103.
[38] O.K. Gasymov, A.R. Abduragimov, B.J. Glasgow, pH-dependent conformational changes in tear lipocalin by site-directed tryptophan fluorescence, Biochemistry 49 (2010) 582–590.
[39] B.J. Glasgow, C. Heinzmann, T. Kojis, R.S. Sparkes, T. Mohandas, J.B. Bateman, Assignment of tear lipocalin gene to human chromosome 9q34-9qter, Curr. Eye Res. 12 (1993) 1019–1023.
[40] B.J. Glasgow, Tissue expression of lipocalins in human lacrimal and von Ebner's glands: colocalization with lysozyme, Graefes Arch. Clin. Exp. Ophthalmol. 233 (1995) 513–522.
[41] B. Cormack, In Current Protocol in Molecular Biology, Greene Pub. Associates and Wiley-Interscience, New York, N.Y., 1987
[42] N. Sreerama, R.W. Woody, Estimation of protein secondary structure from circular dichroism spectra: comparison of CONTIN, SELCON, and CDSSTR methods with an expanded reference set, Anal. Biochem. 287 (2000) 252–260.
[43] S.S. Lehrer, Solute perturbation of protein fluorescence. The quenching of the tryptophyl fluorescence of model compounds and of lysozyme by iodide ion, Biochemistry 10 (1971) 3254–3263.
[44] A. Sillen, Y. Engelborghs, The correct use of “average” fluorescence parameters, Photochem. Photobiol. 67 (1998) 475–486.
[45] J.R. Lakowicz, Principles of Fluorescence Spectroscopy, Third ed.Springer, New York, 2006.
[46] S. Kuppens, M. Hellings, J. Jordens, S. Verheyden, Y. Engelborghs, Conformational states of the switch I region of Ha-ras-p21 in hinge residue mutants studied by fluorescence lifetime and fluorescence anisotropy measurements, Protein Sci. 12 (2003) 930–938.
[47] T. Förster, Ann. Phys. 2 (1948) 55–75.
[48] R.W. Woody, Theory of circular dichroism of proteins, in: G.D. Fasman (Ed.), Circular Dichroism and the Conformational Analysis of Biomolecules, Plenum Press, New York, 1996, p. 55.
[49] C. Chothia, Conformation of twisted beta-pleated sheets in proteins, J. Mol. Biol. 75 (1973) 295–302.
[50] C.P. Pan, P.R. Callis, M.D. Barkley, Dependence of tryptophan emission wavelength on conformation in cyclic hexapeptides, J. Phys. Chem. B 110 (2006) 7009–7016.
[51] J.T. Vivian, P.R. Callis, Mechanisms of tryptophan fluorescence shifts in proteins, Biophys. J. 80 (2001) 2093–2109.
[52] Y. Engelborghs, The analysis of time resolved protein fluorescence in multi-tryptophan proteins, Spectrochim. Acta A Mol. Biomol. Spectrosc. 57 (2001) 2255–2270.
[53] C.P. Pan, M.D. Barkley, Conformational effects on tryptophan fluorescence in cyclic hexapeptides, Biophys. J. 86 (2004) 3828–3835.
[54] Y. Chen, B. Liu, H.T. Yu, M.D. Barkley, The peptide bond quenches indole fluorescence, J. Am. Chem. Soc. 118 (1996) 9271–9278.
[55] B.J. Glasgow, A.R. Abduragimov, T.N. Yusifov, O.K. Gasymov, J. Horwitz, W.L. Hubbell, K.F. Faull, A conserved disulfide motif in human tear lipocalins influences ligand binding, Biochemistry 37 (1998) 2215–2225.
[56] Y. Chen, M.D. Barkley, Toward understanding tryptophan fluorescence in proteins, Biochemistry 37 (1998) 9976–9982.
[57] D.D. Boehr, R. Nussinov, P.E. Wright, The role of dynamic conformational ensembles in biomolecular recognition, Nat. Chem. Biol. 5 (2009) 789–796.
[58] G.G. Hammes, Y.C. Chang, T.G. Oas, Conformational selection or induced fit: a flux description of reaction mechanism, Proc. Natl. Acad. Sci. U. S. A. 106 (2009) 13737–13741.
[59] N. Tokuriki, D.S. Tawfik, Protein dynamism and evolvability, Science 324 (2009) 203–207.
[60] T.R. Weikl, C. von Deuster, Selected-fit versus induced-fit protein binding: kinetic differences and mutational analysis, Proteins 75 (2009) 104–110.
[61] K. Okazaki, S. Takada, Dynamic energy landscape view of coupled binding and protein conformational change: induced-fit versus population-shift mechanisms, Proc. Natl. Acad. Sci. U. S. A. 105 (2008) 11182–11187.
[62] H. Frauenfelder, P.W. Fenimore, R.D. Young, Protein dynamics and function: insights from the energy landscape and solvent slaving, IUBMB Life 59 (2007) 506–512.
[63] F. Vincent, S. Spinelli, R. Ramoni, S. Grolli, P. Pelosi, C. Cambillau, M. Tegoni, Complexes of porcine odorant binding protein with odorant molecules belonging to different chemical classes, J. Mol. Biol. 300 (2000) 127–139.
[64] K. Sakurai, T. Konuma, M. Yagi, Y. Goto, Structural dynamics and folding of beta-lactoglobulin probed by heteronuclear NMR, Biochim. Biophys. Acta 1790 (2009) 527–537.
[65] L. Ragona, F. Fogolari, M. Catalano, R. Ugolini, L. Zetta, H. Molinari, EF loop conformational change triggers ligand binding in beta-lactoglobulins, J. Biol. Chem. 278 (2003) 38840–38846.
[66] H.R. Bosshard, Molecular recognition by induced fit: how fit is the concept? News Physiol. Sci. 16 (2001) 171–173.